AGU PUBLICATIONS

JGR

Journal of Geophysical Research: Biogeosciences

RESEARCH ARTICLE

10.1002/2013JG002420

Key Points:
- SOM turnover and transport was estimated using Bayesian calibration
- Radiocarbon data strongly improved constraint of turnover rate of slow pool
- Predictive simulation showed small increase of soil C stocks in 21st century

Supporting Information:
- Readme
- Figures S1–S16 and Tables S1 and S2

Correspondence to:
Maarten C. Braakhekke,
maarten.braakhekke@bgc-jena.mpg.de

Citation:
Braakhekke, M. C., C. Beer, M. Schrumpf, A. Ekici, B. Ahrens, M. R. Hoosbeek, B. Kruijt, P. Kabat, and M. Reichstein (2014), The use of radiocarbon to constrain current and future soil organic matter turnover and transport in a temperate forest, *J. Geophys. Res. Biogeosci.*, *119*, 372–391, doi:10.1002/2013JG002420.

Received 17 JUN 2013
Accepted 17 DEC 2013
Accepted article online 9 JAN 2014
Published online 28 MAR 2014

The use of radiocarbon to constrain current and future soil organic matter turnover and transport in a temperate forest

Maarten C. Braakhekke[1,2], Christian Beer[1,3], Marion Schrumpf[1], Altug Ekici[1], Bernhard Ahrens[1], Marcel R. Hoosbeek[2], Bart Kruijt[2], Pavel Kabat[2,4], and Markus Reichstein[1]

[1]Max Planck Institute for Biogeochemistry, Jena, Germany, [2]Wageningen University, Earth System Science Group, Wageningen, The Netherlands, [3]Department of Applied Environmental Science and Bolin Center for Climate Research, Stockholm University, Stockholm, Sweden, [4]International Institute for Applied Systems Analysis, Laxenburg, Austria

Abstract We investigated the merits of radiocarbon measurements for estimating soil organic matter (SOM) turnover and vertical transport for a temperate deciduous forest in Germany. Eleven parameters, defining decomposition and transport in the soil carbon model SOMPROF, were estimated using a Bayesian approach based on organic carbon measurements and radiocarbon concentration of SOM and heterotrophic respiration. The addition of radiocarbon data had strong effects on the parameters, most importantly a reduction of the decomposition and production rate of the slowest SOM pool by an order of magnitude, and a similar reduction in advective SOM transport. The modified parameters further led to changes in the partitioning of SOM over the different model pools. The calibration results were subsequently used to perform transient soil carbon projections for the period 1901–2100. These simulations were run with parameter sets from calibrations both with and without radiocarbon. The results show an increase over time of topsoil carbon and a decrease in the subsoil, adding to a net gain overall. Near the end of the 21st century, total carbon stocks stabilize and—for the radiocarbon-constrained model—start to decrease. However, the changes are small compared to the total stocks. The model results for the calibrations with and without radiocarbon are in general quite similar, but the latter shows notably higher heterotrophic respiration fluxes. Constraining the model with radiocarbon yielded only a small reduction of uncertainty for the total carbon stocks, while for the individual depth compartments, the uncertainty was increased.

1. Introduction

Recent studies have called attention to the soil as an important source of uncertainty in the prediction of terrestrial carbon cycling [*Sitch et al.*, 2008; *Jones and Falloon*, 2009; *Arora and Matthews*, 2009; *Todd-Brown et al.*, 2013; *Wieder et al.*, 2013]. For example, based on a reanalysis of results from *Friedlingstein et al.* [2006], *Jones and Falloon* [2009] concluded that the spread of future predicted land carbon storage by earth system models is explained for a large part by varying trajectories of global soil carbon stocks. A similar result was found by *Sitch et al.* [2008] in an intercomparison study of dynamic global vegetation models. Because of the large amount of carbon stored globally in soils, uncertainty in representation of soil carbon cycling in earth system models can propagate to considerable variation in predicted atmospheric CO_2 and climate change.

In the context of climate change, the main purpose of a soil carbon model is to predict carbon storage in and fluxes from the soil in response to environmental factors. Therefore, soil carbon models applied at large scale have typically been calibrated to reproduce observed or at least reasonable carbon stocks and heterotrophic respiration fluxes. Since soil organic matter (SOM) comprises a mixture of materials with different turnover times, it is usually modeled as several pools with different turnover rates. The number of pools varies widely, but most models include at least three SOM fractions in order to adequately represent the spectrum of turnover rates observed in reality [*Manzoni and Porporato*, 2009]. Since each pool requires one or more parameters to characterize its behavior, the degrees of freedom of a soil carbon model increase rapidly with each additional pool. Consequently, measured carbon stocks and fluxes alone are in general not sufficient to estimate all parameters of a multipool soil carbon model. Depending on the number of pools, one or more additional sources of information characterizing the organic matter turnover are required.

In absence of such data, a clear best parameter set may not exist. Instead, there may be one or more large regions in parameter space that yield optimal, or almost optimal, fit to observations [*Braakhekke et al.*, 2013]. Selecting a single parameter set in such a region may result in a model that is right for the wrong reason and gives biased predictions when extrapolated to different conditions [*Medlyn et al.*, 2005; *Beven*, 2006; *Tang and Zhuang*, 2008].

The cosmogenic carbon isotope ^{14}C, generally referred to as radiocarbon, has proven to be an ideal tool for quantifying SOM turnover [*Gaudinski et al.*, 2000; *Trumbore*, 2009]. Because of its relatively constant natural formation rate, the availability of accurate past records of atmospheric concentrations, and its long half-life of 5730 years, it can represent the decomposition rates of the most stable organic matter fractions. Furthermore, the large increase of the atmospheric radiocarbon fraction due to nuclear weapons testing in the 1960s allows it to be used for quantifying decadal turnover rates as well. Hence, it has been used extensively for calibrating and evaluating soil carbon models [*Jenkinson and Coleman*, 1994; *Michalzik et al.*, 2003; *Petersen et al.*, 2005; *Jenkinson and Coleman*, 2008].

Studies in which radiocarbon was measured at multiple levels in the soil profile have shown that SOM generally becomes older with depth [*Trumbore et al.*, 1995; *Rumpel et al.*, 2002; *Schrumpf et al.*, 2013]. It has been suggested that certain mechanisms that cause stabilization of organic matter are comparatively more important in the subsoil [*Rumpel et al.*, 2012]. Examples of such mechanisms include sorption to minerals [*Eusterhues et al.*, 2003], energy or nutrient limitation of microbes [*Fontaine et al.*, 2007; *Fierer et al.*, 2003], and spatial inaccessibility of SOM [*Chabbi et al.*, 2009]. Conversely, the radiocarbon depth gradient may also be explained by vertical transport of SOM. Since transport rates are generally quite low, the time needed for material to reach deeper levels will cause a vertical age gradient [*Kaiser and Kalbitz*, 2012]. Furthermore, downward migration presumably leads to vertical segregation of organic matter, causing slower fractions to become more prominent with depth. The main cause of changes in SOM dynamics along the profile is not well known and presumably differs between sites. However, a multipool soil carbon model will inevitably show decreasing average turnover rates with depth, when combined with vertical transport [*Elzein and Balesdent*, 1995]. This suggests that profile measurements of SOM and radiocarbon may provide additional constraint on turnover rates, if combined with a vertical transport model. On the other hand, since SOM transport rates are poorly known, they need to be estimated in addition, which partially negates the improved constraint on the decomposition parameters.

We aimed to study the merits of radiocarbon measurements for characterizing SOM turnover and vertical transport in a temperate deciduous forest in Germany. To this end, radiocarbon activity of soil organic matter and heterotrophic respiration were used together with organic carbon measurements to estimate parameters of the soil carbon model SOMPROF with a Bayesian calibration approach. SOMPROF [*Braakhekke et al.*, 2011] is a vertically explicit SOM model that simulates the distribution of organic matter over the mineral soil profile and surface organic layers. It is based on simple but explicit representations of bioturbation (mixing by the soil fauna), liquid phase transport, (root) litter input, and decomposition. A previous calibration study for the same site without radiocarbon indicated that the vertical SOM profile can be explained in several ways [*Braakhekke et al.*, 2013]. Here, we used a reduced version of the model and studied how the addition of radiocarbon data affects the parameters by performing calibrations with and without these observations. The calibrations were performed in a Bayesian framework with Monte Carlo inversion, allowing full characterization of parameter distributions and inclusion of prior knowledge. Furthermore, it was studied how the updated parameters and their uncertainty affect predictions of future soil carbon cycling under conditions of climate change. Based on the results of the calibrations, an ensemble of forward simulations until 2100 were run, using litter fluxes and soil climate predicted by the land surface model JSBACH [*Raddatz et al.*, 2007].

2. Methods

2.1. Site Description

The study site is located in a deciduous old-growth forest in the Hainich national park in Germany (51°4′45.36″ N; 10°27′7.20″ E). The climate is temperate subcontinental with an average annual precipitation of 800 mm and average temperature of 7–8°C. The main tree species are beech (*Fagus sylvatica*) and ash (*Fraxinus excelsior*), and the soil is covered by herbaceous vegetation (*Allium ursinum*, *Mercurialis perennis*, *Anemone nemorosa*) from April to October [*Knohl et al.*, 2003]. The main soil type is Cambisol [*IUSS Working Group WRB*, 2007], formed in loess on limestone bedrock with a depth of 50–70 cm. The soils are fertile,

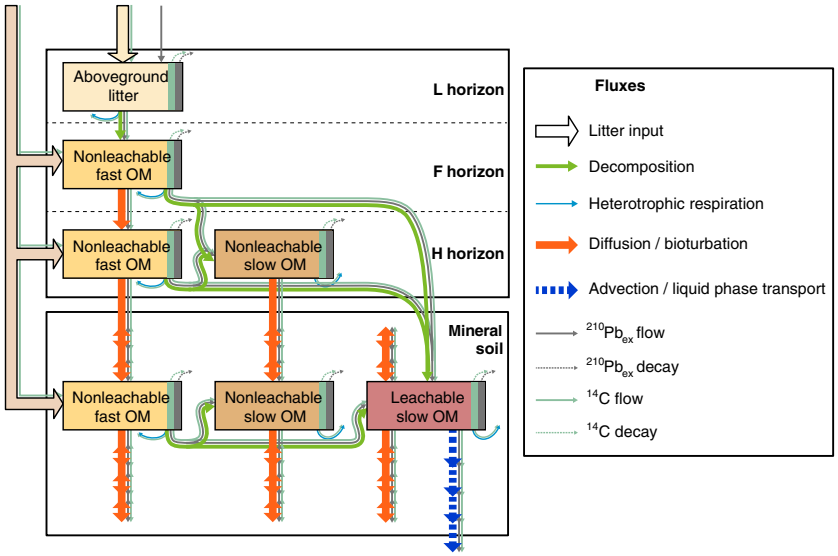

Figure 1. Structure of the SOMPROF model.

with a high clay content (loamy clay texture) and pH (pH-H_2O 5.9–7.8; T. Persson, personal communication, 2011). The humus type is mull with a thin organic layer of 3–5 cm, and a well-developed A horizon of 5–10 cm, indicating a high biological activity and fast decomposition. Approximately 90% of the root biomass occurs above 40cm depth.

Soil temperature and moisture are measured continuously at half-hourly intervals. From this data, average annual cycles of soil temperature and moisture were derived, which were used in the simulations (supporting information Figures S1 and S2). Although there is no permanent water table, soil moisture in the subsoil is persistently higher due to the obstructing effect of the bedrock.

Prior to the establishment of the national park in 1997, the forest was used by the military for approximately 60 years. Hence, the site has been unmanaged for at least 70 years. In the preceding centuries, the forest was used extensively as coppice. Currently, the ages of the trees cover a wide range of up to 250 years. Large amounts of standing dead wood and woody debris on the forest floor attest to the forest's unmanaged character.

2.2. Model Description and Simulation Setup

The SOMPROF model and simulation setup have previously been described elsewhere [*Braakhekke et al.*, 2011, 2013]. Hence, we only provide a general description of the model here and focus on the changes with respect to these publications.

SOMPROF simulates organic carbon stocks and mass fractions in the mineral soil and three surface organic horizons: L, F, and H (Figure 1). The model accounts for organic matter (OM) input by roots and aboveground litter fall, decomposition, and two mechanisms for vertical OM transport: bioturbation (mixing of the soil by the soil fauna) and movement with the liquid phase. The model further includes a module simulating the profile of excess lead-210 ($^{210}Pb_{ex}$), a radiogenic isotope which can be used as a tracer for SOM transport.

The version of SOMPROF used in this study contains four OM pools: aboveground litter (AGL), nonleachable fast organic matter (NLF), nonleachable slow organic matter (NLS), and leachable slow organic matter (LS). Decomposition of the OM pools is simulated as first-order kinetics, controlled by the decomposition rate k (yr^{-1}). The decomposition rate is dependent on soil temperature and moisture but otherwise independent of depth. The decomposition flux is partitioned by transfer coefficients into a fraction (α) that flows to more decomposed pools and a fraction ($1 - \alpha$) that is lost as CO_2 (heterotrophic respiration). Previously, the NLF pool was split into two pools: fragmented litter, which represented fresh litter transformed after a first decomposition step, and root litter, representing organic matter input by roots. In a calibration study [*Braakhekke et al.*, 2013], it was found that the observations could constrain the decomposition rate coefficient for only one of these two pools, which suggests that one of them is redundant. Since the two

pools are very similar in terms of quality and transport behavior, we chose to merge them into the NLF pool since this removes three parameters.

Organic matter input occurs as aboveground litter in the L horizon and over the whole profile due to input from roots as nonleachable fast OM. Root input is vertically distributed according to a function of depth, starting at the top of the F horizon and exponentially declining, determined by a shape parameter β (m^{-1}).

The organic horizons are treated as homogenous connected reservoirs. Decomposition products formed in the L and F layers are assumed to flow to the underlying horizon. Additional downward transport between horizons and into the mineral soil occurs by bioturbation, which is represented as a fixed (zeroth order) downward flux (the bioturbation rate B kg m^{-2} yr^{-1}), distributed over the pools according to their mass fractions. Aboveground litter is the only pool not moved by bioturbation, and as such is only present in the L horizon. Liquid phase transport is not considered for the organic layer: all leachable material is assumed to flow immediately to the mineral soil. In the mineral soil, bioturbation is simulated as a diffusion process, with the diffusivity D_{BT} determined by the bioturbation rate and the mixing length l_m (m) according to

$$D_{BT} = \frac{1}{2}\frac{B}{\rho} l_m , \quad (1)$$

where ρ is the bulk density, which may vary with depth. For the simulations for the calibrations, ρ was based on local measurements, while in the projection simulations (section 2.5), it was determined from the local organic matter fraction using a pedotransfer function from *Federer et al.* [1993]. Transport of organic matter with the liquid phase is only considered for the mineral soil and may lead to loss of organic matter over the lower boundary. It is simulated as an advection process, controlled by the advection rate v (m yr^{-1}). Only the leachable slow organic matter pool is subject to advection. The parameters controlling vertical transport, B, l_m, and v, are all assumed to be constant with depth, although diffusivity may be variable due to bulk density differences.

The simulations for the calibrations covered the period 1810–2009, with monthly time steps. The model was forced by repeated average annual cycles of litter fluxes and soil temperature and moisture, which were derived from in situ measurements [*Braakhekke et al.*, 2013]. Lead-210 input was held constant at 1; the absolute values were not required since both the modeled and measured $^{210}Pb_{ex}$ profile were normalized with respect to the value at the soil surface [*Braakhekke et al.*, 2013]. The depth of the lower boundary was set at 70 cm, which is the approximate depth of the bedrock (see section 2.1). Additional model input is presented in supporting information Table S1. The forcing for the radiocarbon model is discussed below.

In view of the high age of the Hainich forest and the absence of any known major land-use changes in the past (see section 2.1), it was assumed that the soil is in steady state at the start of the simulation, for average constant forcing. A Newton-Raphson root-finding algorithm [*Press et al.*, 1996, Ch. 9] was used to directly estimate the steady state for given parameter values.

2.2.1. Radiocarbon Simulation

Radiocarbon (^{14}C) is a cosmogenic radioisotope formed in the upper atmosphere by interactions between cosmic radiation and atmospheric nitrogen. Additionally, aboveground nuclear weapons testing, mostly during the 1960s, produced a large amount of radiocarbon, roughly doubling the atmospheric activity in less than 10 years (the "bomb-peak"; c.f. supporting information Figure S3). The $\frac{^{14}C}{^{12}C}$ ratio of carbon incorporated in organic tissue is determined by the atmospheric ratio at the time of fixation, as well as fractionation effects due to the mass difference between the isotopes. Since the exchange with the atmosphere ceases after uptake, the radiocarbon activity of fixed carbon is influenced only by radioactive decay and mixing with other organic carbon sources. This allows radiocarbon to be used as a tracer to quantify carbon flows and average turnover rates. Particularly valuable in the context of soil carbon cycling is the combined use of radiocarbon of SOM and of heterotrophic respiration. These two variables contain information on turnover rates of slow and fast fractions, respectively [*Sierra et al.*, 2012].

SOMPROF was extended with a module simulating radiocarbon cycling in soil organic matter (Figure 1). The radiocarbon calculations were based on units of percent modern, corrected for the decay of the standard since 1950 [*Stuiver and Polach*, 1977]. This quantity is directly proportional to the true radiocarbon activity. Measurements and model results are reported as $\Delta^{14}C$, which is more a common unit in soil science. Input of radiocarbon into the soil profile was determined as the product of the litter flux and the atmospheric radiocarbon fraction at a fixed lag period before the simulation time. This lag time accounts for the time spent

Table 1. Measured Variables Used in the Calibration[a]

Name	No. of Depth Increments	Measurement Year(s)	Total No. of Data Points
C stock[b]	3	2004, 2009	60
C fraction[c]	7	2004, 2007	136
Effective decomposition rate coefficient[d]	9	2004	89
Lead-210 activity[c,e]	7	2001	7
Total heterotrophic respiration[f]	1	2000–2007	8
Radiocarbon of SOM	up to 9	2001, 2004, 2009	112
Radiocarbon of heterotrophic respiration[c,d,e]	4	2001	4

[a]Depth increments refer both to layers in the mineral soil as well as organic horizons. Total No. of Data Points represents the sum over all years, depth increments, and replicates. Note that the radiocarbon measurements were only included for calibration wC14.
[b]L, F/H horizons, and total mineral soil.
[c]Only for the mineral soil.
[d]Based on lab incubations.
[e]*Fujiyoshi and Sawamura* [2004].
[f]*Kutsch et al.* [2010].
[g]*Hahn and Buchmann* [2004].

by the carbon in the vegetation. The lag time for root litter was estimated at 8 years, based on literature [*Gaudinski et al.*, 2000] and local radiocarbon measurements of roots (data not shown). For aboveground litter, a lag time of 1 year was used. Several records of atmospheric radiocarbon activity were combined to construct a time series for the radiocarbon fraction of the litter input [*Stuiver et al.*, 1998; *Reimer et al.*, 2004; *Levin and Kromer*, 2004; *Hua and Barbetti*, 2004, I. Levin, personal communication, 2011]. The initial conditions at the start of the simulation were calculated based on a fixed input equal to the average of the last 5000 years before the simulation ($\Delta^{14}C = 10.02‰$). For the simulation period (1810–2009), a time series of variable atmospheric radiocarbon content was used (supporting information Figure S3).

Once present in the soil, radiocarbon follows all flows of organic carbon represented in the model: decomposition, heterotrophic respiration, bioturbation, and liquid phase transport. Additionally, radiocarbon is lost by radioactive decay at a rate of $1.21 \times 10^{-4} yr^{-1}$. For the organic layer, all radiocarbon flows were determined simply by multiplying the organic carbon fluxes from a given pool by its radiocarbon fraction. For the mineral soil, separate partial differential equations were composed for each pool which account for all relevant processes. These equations were solved numerically using the same techniques as used for organic carbon.

2.3. Observations Used in the Calibration

Measurements of seven variables were used in the calibration (Table 1). For several variables, multiple values were included, representing different replicates, depths, or points in time. Model-data fit was calculated for model predictions at the sampling time of the corresponding measurements. Most observations can be expected to have right-skewed distributions since they have a theoretical lower bound at zero and large spatial variance. Therefore, all measurement variables, except lead-210, were log-transformed for the calibration, in order to bring their distributions closer to normal. Since the lead-210 data used here are the fraction in excess to the amount that was formed in situ, this quantity may also be negative [*Braakhekke et al.*, 2013]; hence, it was not log transformed.

C stocks and mass fractions were measured in 2004 and 2009 for up to seven depth levels and 10 replicates [*Schrumpf et al.*, 2011]. Effective decomposition rate coefficients were determined from respired CO_2 during lab incubations of samples taken in 2004 [*Kutsch et al.*, 2010]. Measurements of lead-210 activity were taken from *Fujiyoshi and Sawamura* [2004] and were normalized and corrected for in situ formed lead-210, as described in *Braakhekke et al.* [2013]. Total average heterotrophic respiration for the years 2000–2007 was taken from *Kutsch et al.* [2010] who estimated it using field measurements of soil respiration and a model for autotrophic respiration. Radiocarbon measurements of both SOM and heterotrophic respiration in 2001 were taken from *Hahn and Buchmann* [2004]. Additionally, measurements of radiocarbon of SOM for 2004 and 2009 were included (M. Schrumpf et al., Single-pool models underestimate exchange of old for new organic carbon in forest topsoils, in prep.).

Table 2. The Model Parameters Estimated in the Calibration[a]

Parameter	Symbol	Units	Prior Distribution	Upper Bound
Decomposition Rate Coefficients at 10°C and Optimal Soil Moisture				
Aboveground litter	k_{AGL}	yr^{-1}	$\text{Log}-\mathcal{N}(-0.23, 0.74)$	3
Nonleachable fast OM	k_{NLF}	yr^{-1}	$\text{Log}-\mathcal{N}(-0.23, 0.74)$	3
Nonleachable slow OM	k_{NLS}	yr^{-1}	$\text{Log}-\mathcal{N}(-2.23, 1.00)$	3
Leachable slow OM	k_{LS}	yr^{-1}	$\text{Log}-\mathcal{N}(-2.23, 1.00)$	3
Transfer Coefficients				
Aboveground litter–nonleachable fast OM	$\alpha_{AGL\rightarrow NLF}$	-	$\text{Logit}-\mathcal{N}(0.43, 0.95)$	1
Nonleachable fast OM–nonleachable slow OM	$\alpha_{NLF\rightarrow NLS}$	-	$\text{Logit}-\mathcal{N}(-0.93, 0.98)$	$1, \left(1-\alpha_{NLF\rightarrow LS}\right)$
Nonleachable fast OM–leachable slow OM	$\alpha_{NLF\rightarrow LS}$	-	$\text{Logit}-\mathcal{N}(-0.93, 0.98)$	$1, \left(1-\alpha_{NLF\rightarrow NLS}\right)$
Transport Parameters				
Bioturbation rate	B	$kg\ m^{-2}\ yr^{-1}$	uniform	3
Mixing length	l_m	m	uniform	3
Liquid phase transport (advection) rate	v	$m\ yr^{-1}$	uniform	0.1
Shape parameter for root litter input profile	β	m^{-1}	$\mathcal{N}(7, 1.2)$	14

[a]The lower bound for all parameters is zero; the upper bound is given in the table.

2.4. Bayesian Calibration

Eleven model parameters were estimated: seven parameters related to decomposition, three parameters related to transport, and one parameter quantifying the vertical distribution of root litter input (Table 2).

The calibrations were performed in two setups: without radiocarbon observations (woC14) and with radiocarbon observations (wC14), using a Bayesian approach. Bayesian calibration is aimed at deriving the posterior distribution: a multivariate distribution of the model parameters, conditional on prior knowledge, the model structure, and the observations. The posterior is defined (up to a constant) as the product of prior distribution $p(\boldsymbol{\theta})$, which expresses knowledge about the model parameters $\boldsymbol{\theta}$ prior to the calibration, and the likelihood function $p(\mathbf{O}|\boldsymbol{\theta})$, which defines the probability of the measurements $\mathbf{O}$, given model parameters $\boldsymbol{\theta}$ [*Gelman et al.*, 2004]:

$$p(\boldsymbol{\theta}|\mathbf{O}) \propto p(\boldsymbol{\theta})\, p(\mathbf{O}|\boldsymbol{\theta}). \tag{2}$$

The posterior distributions were approximated with a Markov Chain Monte Carlo approach using the DREAM(ZS) algorithm [*Laloy and Vrugt*, 2012]. Additional information about the calibration can be found in the Appendix.

2.4.1. Likelihood Function

The observations used in the study comprised several "data streams", i.e., variables for which the distribution of the model-data residuals is expected to be different. Measurements at different horizons/depth levels were considered part of the same data stream, while measurements at different time points were treated as separate data streams. The overall likelihood was defined as the product of the likelihoods for all individual data streams:

$$p(\boldsymbol{\theta}|\mathbf{O}) = \prod_{i=1}^{I} p_i(\mathbf{O}_i|\boldsymbol{\theta}), \tag{3}$$

where I is the total number of data streams. As implied by equation (3), correlations between data streams were not considered. For all data streams a Gaussian likelihood function was used. For a data stream i with N_i data points, the conditional likelihood function for given $\boldsymbol{\theta}$ and standard deviation σ_i is defined as

$$p(\mathbf{O}_i|\boldsymbol{\theta}, \sigma_i) \propto \sigma_i^{-N_i} \exp\left(-\frac{1}{2\sigma_i^2} SS_i(\boldsymbol{\theta}, \mathbf{O}_i)\right). \tag{4}$$

$SS_i(\boldsymbol{\theta}, \mathbf{O}_i)$ is the sum of squared residuals for data stream *i*:

$$SS_i(\boldsymbol{\theta}, \mathbf{O}_i) = \sum_{n=1}^{N_i} (O_{i,n} - M_i(\boldsymbol{\theta}))^2, \tag{5}$$

where $O_{i,n}$ is the measured value for replicate *n* and $M_i(\boldsymbol{\theta})$ is the model prediction for parameters $\boldsymbol{\theta}$. Replicate measurements, when available, were all included individually in $SS_i(\boldsymbol{\theta})$, which means that single model predictions were compared to several observed quantities. The standard deviation of the model–data residuals σ_i depends on both measurement and modelling related errors and is usually not known a priori. It may be estimated as an additional parameter during the calibration [*Gelman et al.*, 2004], but since we are not particularly interested in σ_i, an expedient approach is to remove it from the likelihood function by integration [*Kavetski et al.*, 2006]. The resulting likelihood function represents the distribution of the residuals marginalized over all values of σ_i. For all data streams, we chose the uninformative Jeffreys prior for σ_i ($p(\sigma_i) \propto \frac{1}{\sigma_i}$). This yields the following formulation for the marginal likelihood function:

$$p(\mathbf{O}_i|\boldsymbol{\theta}) = SS_i(\boldsymbol{\theta}, \mathbf{O}_i)^{-\frac{N_i}{2}}. \tag{6}$$

2.4.2. Prior Distributions

Since the current study includes the data used by *Braakhekke et al.* [2013], we used the same prior distributions (except for the shape parameter for root litter input, which was previously not included). The distributions were chosen relatively broad in order to give freedom to the parameters. Lognormal priors were used for the decomposition rates and transport parameters, which are bounded at zero. For the transfer coefficients, we used a logit-normal function, which is similar to the beta distribution and bounded between zero and one [*Mead*, 1965]. Furthermore, the sum of $\alpha_{\mathrm{NLF}\rightarrow\mathrm{NLS}}$ and $\alpha_{\mathrm{NLF}\rightarrow\mathrm{LS}}$ was limited to 1. The prior distributions are based on knowledge from previously published studies [see, e.g., *Braakhekke et al.*, 2011], as well as the following assumptions: (i) parameter distributions are skewed away from the (nearest) bound [see *Braakhekke et al.*, 2013], (ii) the probability density approaches zero near a bound, (iii) the NLS and LS pools are more recalcitrant than AGL and NLF pools (i.e., *k* is lower), and (iv) the fraction of the decomposition flux that is lost as CO_2 is larger (i.e., α is lower) for the NLS and LS pools than for the AGL and NLF pools. Point (ii) is not strictly necessary since the model would still be plausible for, e.g., $k_{\mathrm{NLF}} = 0$ or $\alpha_{\mathrm{NLF}\rightarrow\mathrm{NLS}} = 1$. However, the assumption is that all fluxes and pools in the model structure are relevant and should be nonzero.

For the shape parameter of the root litter input depth function (β), we assumed that the mean is sufficiently far away from zero that a normal distribution can be used. The mean was set at 7 m^{-1}, which is the approximate value for root biomass profile at Hainich.

The priors are specified in Table 2 and depicted together with the posterior distributions in Figure 2.

2.5. Projection Simulations

In order to study soil carbon cycling under conditions of climate change, we performed model projections for the period 1901–2100 for the same site, based on the calibration results. For both calibration setups, an ensemble of 500 model simulations was run with parameter sets selected in regular intervals from the posterior sample (see Appendix). The setup of these simulations was identical to those made for the calibrations, with the exception that the mineral soil bulk density was calculated based on the modeled organic matter fraction, instead of measurements.

The forcing variables for the simulation projections (above/belowground litter flux, soil moisture, and soil temperature) were obtained from a simulation run with the ecosystem model JSBACH. Part of the MPI earth system model, JSBACH, simulates land-atmosphere exchange of energy, water, and carbon dioxide [*Raddatz et al.*, 2007; *Brovkin et al.*, 2009]. Its representation of canopy processes such as photosynthesis, respiration, and transpiration is based on the BETHY model [*Knorr*, 2000], with several extensions to represent phenology and carbon cycling [*Raddatz et al.*, 2007], and soil freeze-thaw processes [*Ekici et al.*, 2013].

The simulation with JSBACH model was performed as follows. Vegetation carbon pools were brought to equilibrium by a 1000-year spin-up procedure using 1901–1930 climate and atmospheric carbon dioxide

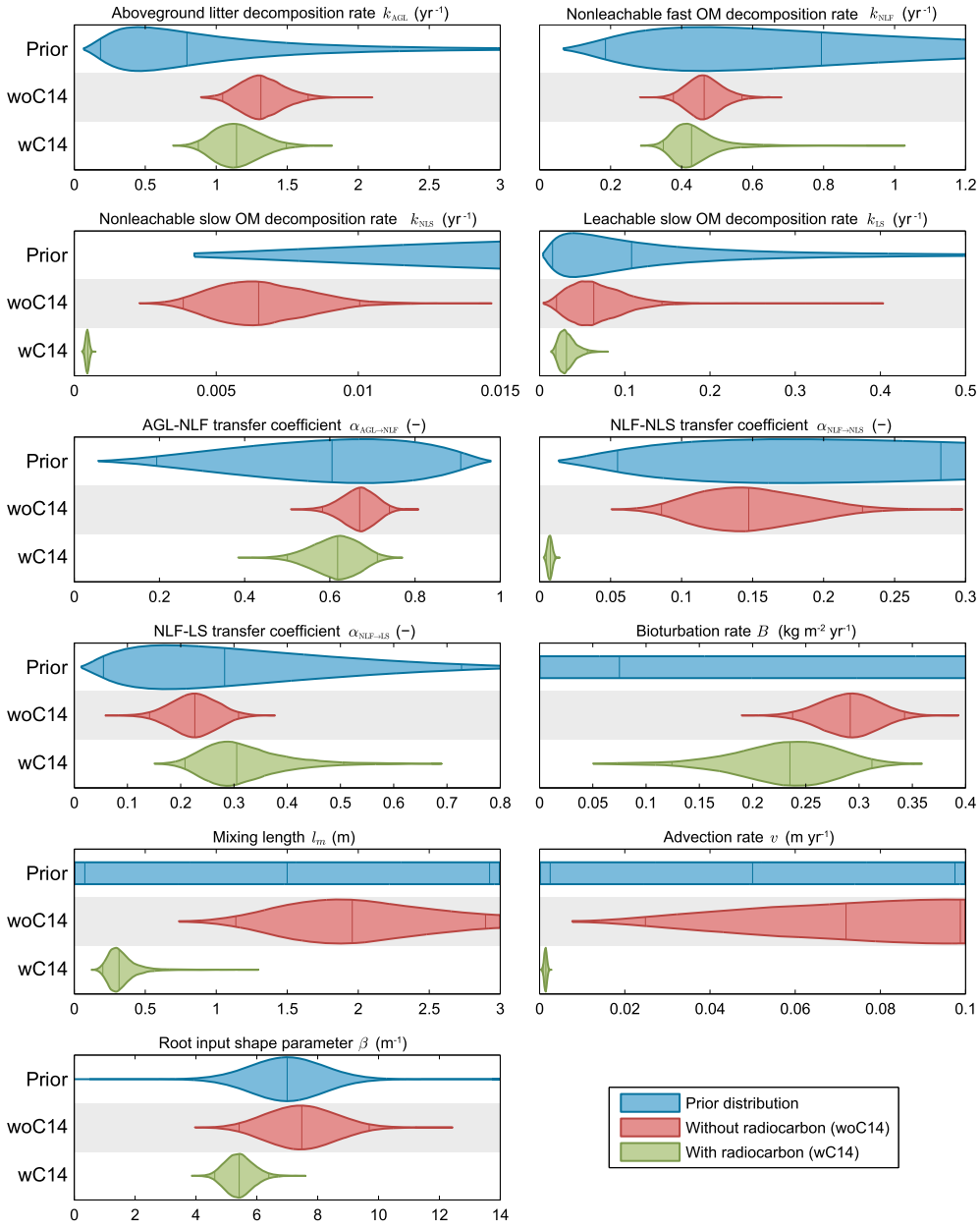

Figure 2. Violin plots of the marginal prior and posterior distributions. The three vertical lines inside the violins indicate the median and the 95% confidence bounds.

concentration for 1901 (296 ppm). Next, the model was run with transient climate and CO_2 for the period 1901–2100. The global atmospheric carbon dioxide concentration followed the CMIP5 protocol [*Meinshausen et al.*, 2011]. The 1901–2100 climate data set consisted of WATCH forcing data [*Weedon et al.*, 2010] for the period 1901–1978, bias-corrected ERA-Interim data [*Dee et al.*, 2011] for the period 1979–2010, and a bias-corrected outputs from the regional climate model KNMI-RACMO for the period 2011–2100. KNMI-RACMO results come from the ENSEMBLES multimodel scenario experiment [*Christensen et al.*, 2008]. For this experiment, the model was driven by lateral boundary conditions derived by the ECHAM5 model, based on the SRES A1B greenhouse gas and aerosol scenario. Bias correction was applied to the ERA-Interim and RACMO results based on the overlapping time period (1979–2010), according to *Piani et al.* [2010], in order to ensure a consistent time series (C. Beer et al., Harmonized long-term climate data for assessing the effect of changing variability on land-atmosphere CO_2 fluxes, in rev. for *Journal of Climate*).

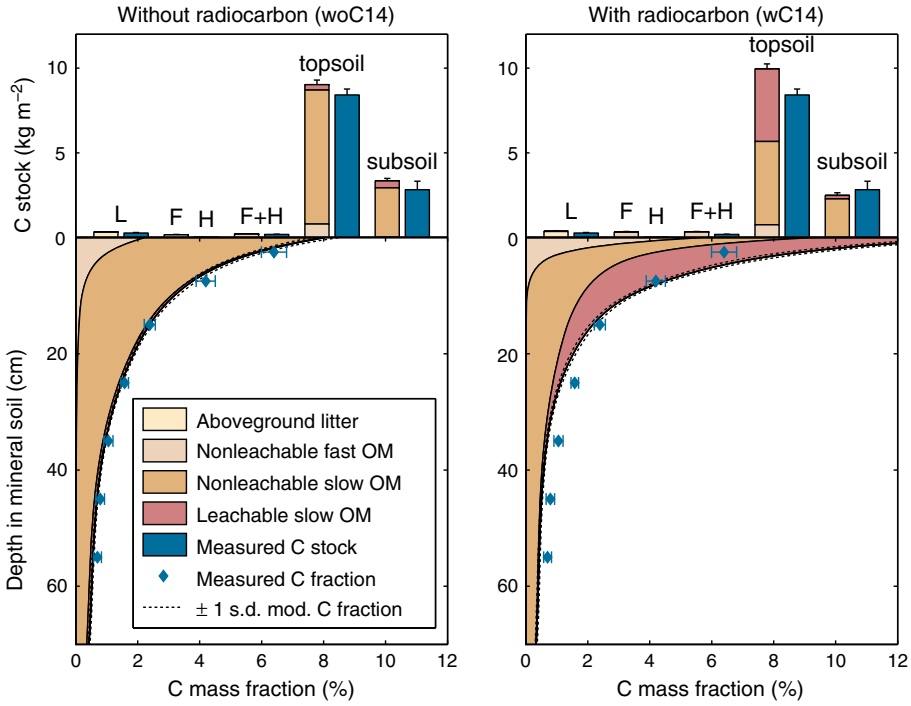

Figure 3. Organic carbon measurements and corresponding model results. L, F, and H refer to the organic horizons (see section 2.2); topsoil: 0–30 cm; subsoil: > 30 cm; OM: organic matter. All model results are ensemble means; error bars denote one standard error of the mean for the measurements and one standard deviation (s.d.) for the model results.

3. Results

3.1. Calibration

3.1.1. Posterior Distribution

Both the calibration setup without radiocarbon (woC14) and with radiocarbon (wC14) yielded a multimodal posterior distribution with two relevant optima. One of the modes performed clearly better in terms of the maximum posterior density. We focus on this mode for discussing the results. The posterior distribution and model predictions for the subdominant mode are presented in the supporting material (Figures S11–S16).

Figure 2 shows the marginal distributions for the prior and the posterior of both calibration setups. Compared to the prior, the uncertainty of all parameters was reduced, already without including radiocarbon data. Adding radiocarbon data led to further constraint for most of the parameters, with the exception of k_{AGL}, $\alpha_{AGL\rightarrow NLF}$, $\alpha_{NLF\rightarrow LS}$, and B. Particularly strong changes are apparent for parameters related to the nonleachable slow (NLS) organic matter pool. The mean decomposition rate coefficient (k_{NLS}) is reduced from 5.7×10^{-3}yr^{-1} to 4.4×10^{-4}yr^{-1} (supporting information Table S2), corresponding an increase of turnover time from roughly 150 year to 2000 year. Additionally, the flow from nonleachable fast (NLF) organic matter to NLS, as determined by $\alpha_{NLF\rightarrow NLS}$, is strongly reduced. Hence, NLS is formed at a lower rate, but it is also more stable. Also, the variance of k_{NLS} and $\alpha_{NLF\rightarrow NLS}$ is an order of magnitude lower when radiocarbon is included. However, the width of these distributions should be considered relative to the mean, since the two are likely correlated over different calibrations. Hence, it is more appropriate to compare the coefficient of variation (standard deviation relative to the mean) which shows a reduction by a factor of around 2 for the two parameters.

A further prominent difference between the two calibrations is apparent for the advection rate v. When radiocarbon is omitted, v has a wide distribution with the marginal mode at the upper bound, whereas with radiocarbon data, v is strongly constrained at the lower end of the range.

3.1.2. Model Results

Figure 3 shows modeled and measured soil carbon stocks and profiles in March 2009. In both calibration setups, the total simulated C stocks and mass fractions are well constrained, having less spread than the

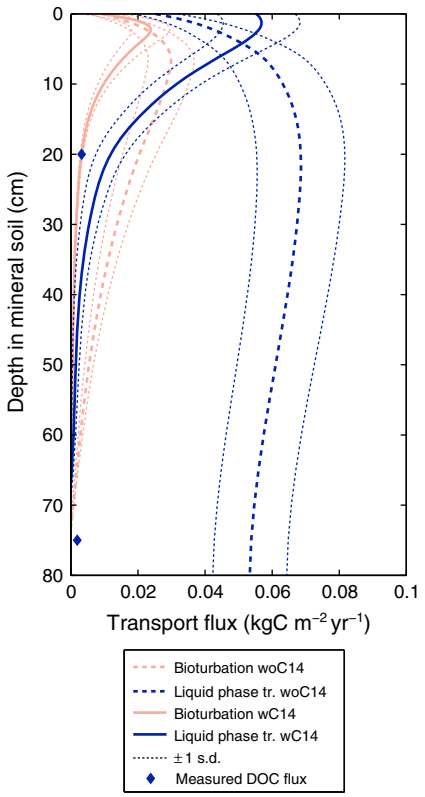

Figure 4. Simulated and measured organic carbon transport fluxes. Model results are ensemble means averaged over the last simulation year. Measured DOC fluxes (not used in the calibration) were taken from *Kindler et al.* [2011].

observations. Addition of radiocarbon led to a decreased fit to observed carbon stocks and mass fractions. The vertical organic carbon distribution became shallower, with overestimated stocks in the organic layer and topsoil and underestimated stocks in the subsoil. Further, the distribution over the different model pools in the topsoil changed, with leachable slow (LS) organic matter becoming more prominent.

Strong differences between the two calibrations are also apparent for the modeled organic matter transport fluxes by bioturbation (diffusion) and liquid phase transport (advection) (Figure 4). Addition of radiocarbon led to a reduction of the flux rates of both mechanisms, which can be attributed to the reduced values of B, I_m, and v. We additionally plotted in situ measured dissolved organic carbon (DOC) fluxes from *Kindler et al.* [2011]. These measurements were not included in the calibration, since the representation of liquid phase transport flow in SOMPROF was not intended for simulation of DOC. However, the simulated advective flux should roughly correspond to DOC transport. Although the advective flux is still overestimated compared to the observations, the strong reduction in flow due to radiocarbon addition is a clear improvement.

Figure 5 shows the measured and modeled radiocarbon activities for both organic matter and heterotrophic respiration. Measured radiocarbon activity of SOM in the mineral soil shows a clear negative gradient, indicating that SOM age increases with depth. The model predicts a similar profile but underestimates the radiocarbon activity in the deep soil. Measured radiocarbon activity of heterotrophic respiration is always higher than that of SOM, which shows that respired carbon is younger than the average total organic matter. Similar to SOM, radiocarbon activity of respired CO_2 decreases with depth. Modeled radiocarbon activity of heterotrophic respiration generally agrees with the observations, although the peak at 10 cm in the modeled vertical profile is not present for the measurements.

Figure 5 further shows strong differences between the radiocarbon profiles of the organic matter pools. These differences are mostly explained by the decomposition rates of the pools, as well as their transport behavior. NLS has markedly lower radiocarbon activity than the other two pools in the mineral soil, indicating it contains on average much older carbon. The profile of LS shows a clear maximum around 8 cm depth, which is caused by the bomb peak travelling downward through the profile. Contrary to the other pools, nonleachable fast (NLF) organic matter shows almost no vertical gradient in the mineral soil, since it originates mostly from root input, which has the same radiocarbon signal throughout the profile. Since NLS and LS are the most abundant pools in the mineral soil, these pools determine the radiocarbon signature there, with the importance of NLS increasing with depth. In contrast, the radiocarbon activity of heterotrophic respiration is determined mostly by the LS pool and, near the surface, by NLF.

3.2. Projection Simulations

The JSBACH ecosystem model predicts both increasing litter fluxes and soil temperatures (Figure 6). Changes in temperature were similar throughout the whole profile. While temperatures keep rising throughout the simulation, litter fluxes stabilize near the end of the century. Soil moisture did not change notably during the simulation period. Already at the start of the simulation in 1901, the litter fluxes calculated by JSBACH are markedly higher than the in situ measurements used in the calibration (c.f. supporting

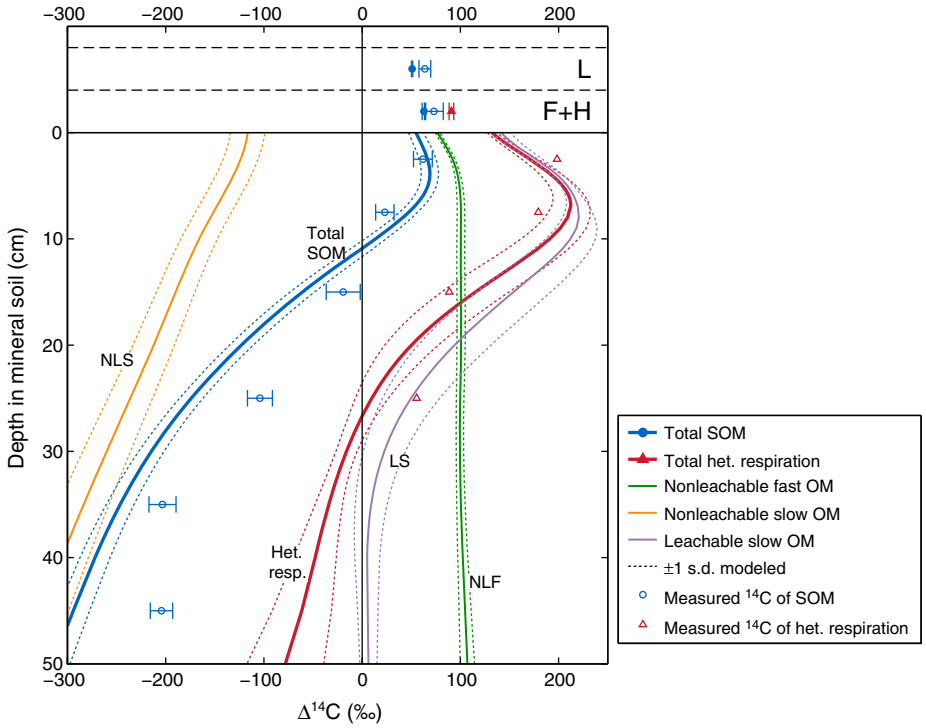

Figure 5. Modeled and measured $\Delta^{14}C$ for organic matter (March 2009) and heterotrophic respiration (April 2001). Model results are means and standard deviation over the simulation ensemble based on parameters from calibration wC14. Measured $\Delta^{14}C$ of heterotrophic respiration were taken from *Hahn and Buchmann* [2004]. Additionally, the $\Delta^{14}C$ values of the individual model pools (March 2009) are depicted. Note that the comparability between the OM $\Delta^{14}C$ and respiration $\Delta^{14}C$ is limited because they are shown for different years.

information Table S1). As a result, also the predicted soil carbon stocks based on the JSBACH forcing are higher than observations (supporting information Figure S10). However, for reasons discussed in section 4.2, we did not correct the JSBACH litter fluxes. Rather than the absolute quantities, we focus on the relative change of simulated carbon stocks over time.

Since the strongest changes in temperature and litter fluxes occur between 1980 and 2100, we limit the discussion of the results to this period. For both calibrations, the simulated organic carbon stocks for the complete profile grow initially. During the second half of the 21st century, the carbon stocks level off and, for simulation wC14, start to decrease (Figures 7a and 7b). However, the overall soil carbon gain is mainly caused by the topsoil; in the subsoil, stocks are in fact decreasing. The simulated total C stock for the two calibration setups diverge over time, with stocks growing faster for simulation woC14 than for wC14. Again, these differences are mainly explained by changes in the topsoil. The relative predictive uncertainty of the C stocks is depicted in Figure 7c as the coefficient of variation over the ensemble. Surprisingly, adding radiocarbon data to the calibration caused an *increase* of the relative uncertainty for the topsoil and subsoil and organic layer, individually. In contrast, the uncertainty for the total soil C stock is slightly reduced (standard deviation in 2100: 0.614 kg m^{-2} for calibration woC14 and 0.525 kg m^{-2} for calibration wC14).

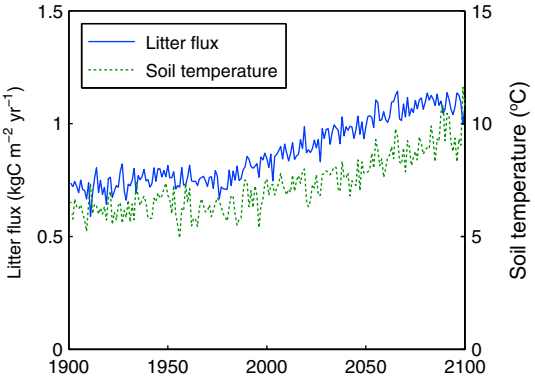

Figure 6. Annual total litter fluxes (aboveground + belowground) and average soil temperature at 8 cm depth at Hainich between 1901 and 2100, simulated by the JSBACH land surface model.

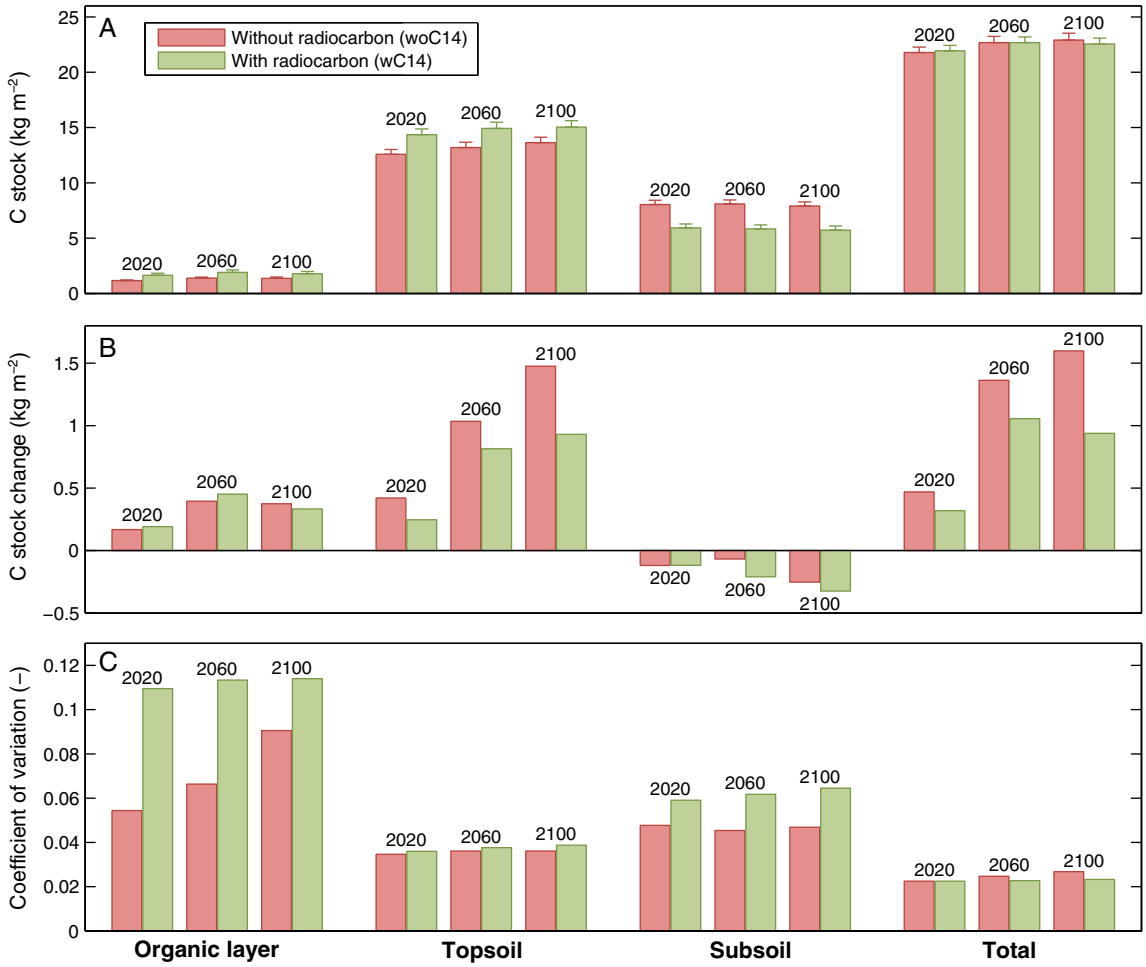

Figure 7. Soil carbon projections based on JSBACH predictions. (a) Total soil C stocks including 95% confidence bounds. (b) Change in C stocks relative to values in 1980. (c) Coefficient of variation (standard deviation relative to mean) over the ensemble for the C stocks.

Figure 8 shows the simulated heterotrophic respiration flux. The average respiration became notably higher (approximately 10%) due to the addition of radiocarbon data. Furthermore, the uncertainty of the simulated flux is strongly reduced by roughly 90%.

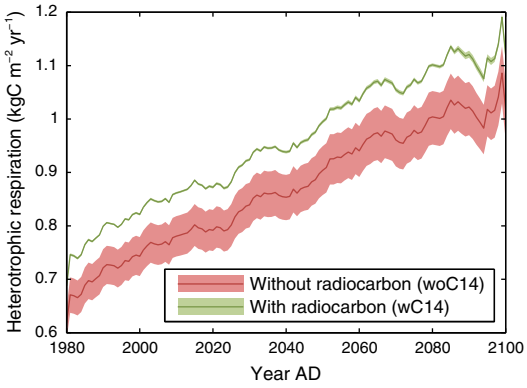

Figure 8. Heterotrophic respiration fluxes for the projections based on JSBACH predictions. The shaded areas indicated the 95% confidence range. The data was smoothed using a 10 year moving average window.

4. Discussion

4.1. Calibration

As mentioned earlier, the posterior distribution for both calibrations has two major optima. A similar result was obtained previously by *Braakhekke et al.* [2013], who found three relevant modes (the two modes found here correspond approximately to modes A and B in *Braakhekke et al.* [2013]). The modes differ markedly in the distribution of SOM over the different pools and transport flux rates (supporting information Figures S12–S14). Conversely, the predicted stocks in the projection simulations are quite similar (supporting information Figure S15). The mode for which we

present the results above has a consistently better fit in both calibrations (log posterior density difference of ~7 and ~10 for calibration woC14 and wC14, respectively), as well in several other setups that were tried. However, it is likely that the performance difference is overestimated since a number of uncertainty sources were not considered, most notable the forcing history and possible deviations from the steady state (see section 4.3). Furthermore, the log posterior density is partially determined by the prior distribution, which is subjective. Future efforts should focus on integrating additional observations that may help to identify the correct mode, such as physical and chemical SOM fractions.

The remainder of the discussion focusses on the dominant mode. The addition of radiocarbon data to the calibration caused major changes in the posterior distribution (Figure 2). For several parameters (k_{NLS}, $\alpha_{NLF\rightarrow NLS}$, I_m, and v), there is virtually no overlap between the marginal distributions of both calibration setups, which indicates that the radiocarbon data are to some extent inconsistent with the other sources of information. Analysis of the different terms of the likelihood function shows a reduced fit to the mineral organic carbon mass fractions and the total heterotrophic respiration for the calibration with radiocarbon data (wC14). This is also apparent from graphical inspection of these variables (Figure 3 and supporting information Figure S6). More important, however, is the increased disagreement with the prior distributions for k_{NLS} and $\alpha_{NLF\rightarrow NLS}$. Our prior estimates for these parameters are markedly higher than the values indicated by the data.

These differences raise the question to what extent posterior is constrained by the prior at low values for these parameters, since the lognormal and logit-normal distributions approach zero probability toward zero. To asses this, an additional calibration with uniform (flat) priors was performed. The results (supporting information Figures S8 and S9) show that the informative priors cause a slight upward shift of the posterior for k_{NLS} and $\alpha_{NLF\rightarrow NLS}$ but have no major effects. Nevertheless, in the future different prior distributions may be considered. As discussed in section 2.4.2, our choice for the lognormal and logit-normal priors is mainly motivated by the assumption that all fluxes and pools in the model are nonzero. If this assumption is relaxed, a prior density function with nonzero probability at zero is appropriate, e.g., exponential or truncated normal.

Interestingly, for some parameters the marginal distributions became wider when radiocarbon data were added. This seems counter intuitive: additional information leads to more uncertainty. The explanation lies in the fact that correlations between parameters are stronger for calibration wC14 (supporting information Figure S4). This demonstrates the importance of considering the correlation structure when assessing the information gain and when selecting a parameter set for forward simulations [*Tang and Zhuang*, 2008].

The addition of radiocarbon data to the calibration led to the introduction of a highly stable organic matter pool, turning over on millennial time scale. Also in previous studies it was found that a passive pool is required in order to reproduce measured radiocarbon activity [*Perruchoud et al.*, 1999; *Gaudinski et al.*, 2000; *Petersen et al.*, 2005; *Koarashi et al.*, 2012]. For example, the inert organic matter (IOM) pool in the soil carbon model RothC is included primarily in order to reproduce observed radiocarbon ages [*Falloon et al.*, 2000]. Compared to similar studies with vertically explicit models [*Elzein and Balesdent*, 1995; *van Dam et al.*, 1997; *Baisden et al.*, 2002], our estimate of the slowest turnover rate is somewhat higher but in the same order of magnitude.

The measured radiocarbon data show a negative depth gradient in the mineral soil (Figure 5). This gradient need not necessarily be caused by a change in average turnover rates with depth. Due to the time needed for vertical transport, also a homogenous SOM pool will show an age—and thus a radiocarbon—gradient with depth (c.f. the radiocarbon profile of NLS, Figure 5). However, apparently this mechanism alone cannot explain the observed profile. Since decomposition rates are not explicitly reduced with depth, additionally a change in the mixing ratio of the SOM pools with depth is required. This presumably explains the increased abundance of the leachable slow (LS) organic matter pool in the topsoil (Figure 3) and improved constraint of the advection rate v, for calibration wC14.

In several similar previous studies, decomposition rates were explicitly decreased along the profile using a depth dependent rate modifier [e.g., *van Dam et al.*, 1997; *Jenkinson and Coleman*, 2008; *Koven et al.*, 2013]. However, *Elzein and Balesdent* [1995] could satisfactorily reproduce observed radiocarbon profiles using only selective preservation of recalcitrant compounds in combination with transport. Therefore, we chose to keep the decomposition rate coefficient constant with depth. Changing SOM dynamics along the vertical

profile is presumably something that needs to be better accounted for, but we believe that it is preferable to explicitly represent the processes and interactions thought to be responsible for this, e.g., organo-mineral interactions or energy-limitation of microbes. However, this is outside the scope of the current study.

Both the measured and modelled radiocarbon profiles display a maximum below the surface, which is caused by the spike in the atmospheric radiocarbon activity due to nuclear weapons testing in 1964 (the bomb peak). This peak causes a similar maximum in the vertical profile which is reduced and travelling downward over time due to organic matter transport. In the modeled profile, the peak is located at approximately 4 cm depth in the mineral soil, while for the measurements, the peak appears to be still in the F/H horizon. This suggests that the vertical organic matter transport is overestimated by the model. The modeled radiocarbon profile of heterotrophic respiration also displays a peak, located somewhat deeper (~6cm), indicating that labile organic matter is transported faster than the slow pools. However, for the measured radiocarbon activity of heterotrophic respiration, the peak is absent. This may indicate that decomposition of root derived material is more important than shown by the model. On the other hand, no replicates were available for these measurements and the lab incubations may not be fully representative for in situ conditions (see section 4.3).

4.2. Projection Simulations

4.2.1. Simulated Soil Carbon Dynamics

As discussed in section 3.2, the litter fluxes predicted by JSBACH are markedly higher than estimates based on in situ measurements [*Kutsch et al.*, 2010], causing a likewise overestimation of stocks in the soil carbon projections. An additional experiment for which the litter fluxes were corrected showed more realistic carbon stocks. However, we chose to show only the original results without correction, for several reasons. First, more than in absolute quantities we are interested in the *relative* SOM dynamics, which change only marginally when litter fluxes are adjusted downward. Second, the current study was performed with future large-scale gridded simulations in mind in which the two models are coupled. In such applications, correction of fluxes based on local measurements would be infeasible and undesirable, since it would lead to disappearance of carbon from the system, rendering the net ecosystem fluxes meaningless.

The JSBACH model predicts both increasing soil temperatures and litter fluxes for the period 1901–2100 (Figure 6), the latter caused by increased vegetation productivity due to CO_2 fertilization. These two trends affect soil carbon stocks in opposite directions. However, while the litter input fluxes level off near the end of the simulation, the temperatures keep rising. This is reflected by the dynamics of the total soil carbon projections (Figure 7): the net balance decreases in the second of half of the 21st century and, for calibration wC14, turns negative. Similar future trajectories with initial carbon uptake, followed by levelling off or carbon loss, have been predicted in global simulation studies [*Cramer et al.*, 2001; *Sitch et al.*, 2008; *Friedlingstein et al.*, 2006; *Jones and Falloon*, 2009].

The simulated soil carbon stocks (Figure 7b) further suggest that the soil at Hainich is currently gaining carbon, which agrees with previous studies based on repeated inventories [*Kutsch et al.*, 2010; *Tefs and Gleixner*, 2012; M. Schrumpf et al., Soil organic carbon and total nitrogen gains in an old growth deciduous forest in Germany, in rev. for *PlosOne*]. Notwithstanding, there are several unconsidered sources of uncertainty that potentially affect the simulated soil carbon stocks. First, neither SOMPROF nor the version of JSBACH used in this study considers nitrogen cycling. It has been suggested that vegetation models that ignore nitrogen limitation on productivity may overestimate carbon sequestration due to climate change [*Hungate et al.*, 2003]. On the other hand, nitrogen deposition may lead to reduced heterotrophic respiration and soil carbon sequestration [*Janssens et al.*, 2010]. Second, due to insufficient data availability, the temperature sensitivity of decomposition was not included in the calibration but held fixed at the value reported by *Lloyd and Taylor* [1994]. There is still little consensus regarding exact temperature sensitivity [*Davidson and Janssens*, 2006], which causes considerable uncertainty of predicted future soil carbon stocks [*Jones and Falloon*, 2009].

Interestingly, the topsoil and the subsoil show opposite response to changes in forcing: topsoil C stocks increase, while subsoil C stocks decrease. Clearly, the increased carbon input remains mostly near the surface, while at deeper levels, net losses occur due to accelerated decomposition. Whether this would also occur in reality for the given conditions is difficult to ascertain. Several mechanisms that may influence the SOM dynamics as a function of depth are currently not represented in the model since they are poorly understood. First, all SOM pools in the model have the same response function for temperature. In reality

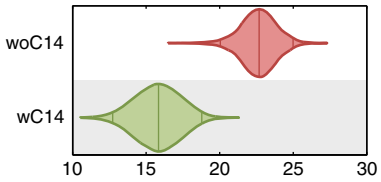

Figure 9. Posterior distribution for the ratio of $\alpha_{NLF \rightarrow NLS}$ and k_{NLS} for the two calibrations.

the temperature sensitivity of decomposition may differ among different organic matter fractions, although this is still uncertain [*Conant et al.*, 2011]. Second, it has been shown that increased input of fresh litter in the subsoil may destabilize old SOM due to priming of microbial activity [*Fontaine et al.*, 2007]. Third, increased belowground productivity may lead to deeper root distributions [*Iversen*, 2010], causing also deeper input of SOM. Nevertheless, these results demonstrate that different parts of the SOM profile can respond differently to environmental changes. Thus, topsoil carbon dynamics should not be simply extrapolated downward in order to derive changes in the subsoil.

4.2.2. Differences Between Calibrations

An important difference between the two calibrations lies in the predicted loss of carbon over the lower boundary by advection (Figure 4), which is unrealistically high for calibration woC14—up to 20% of the litter input. The smaller advective flux rates for wC14 also constitute a strong improvement compared to measured DOC fluxes. A further consequence is the markedly higher heterotrophic respiration flux (Figure 8). This is explained by the steady state assumption applied in the calibration: since carbon leaching is reduced, respiration much increase in order to maintain zero net carbon balance. Interestingly, compared to the observations, heterotrophic respiration is overestimated in calibration wC14 (supporting information Figure S6). This suggests that the steady state assumption is incorrect and that the soil is in fact gaining carbon, which is in agreement with the simulated soil carbon stocks (Figure 7b). The relative contributions of advection and respiration to the total loss are highly relevant for soil carbon dynamics under climate change, because the latter is sensitive to temperature while the former is not. This presumably also explains why calibration wC14 shows stronger carbon losses near the end of the projection simulation. Parameter sets applied for predictive simulations should produce realistic advective losses in order to avoid biased results.

An unexpected result is the larger spread for the carbon stocks in the organic layer, topsoil, and subsoil individually, in calibration wC14 (Figure 7c). Remarkably, adding information to the calibration led to an increase of predictive uncertainty for these variables. Conversely, for the *total* profile, the uncertainty was slightly reduced. This indicates that the vertical distribution of SOM became more uncertain. A further explanation may lie in the fact that the predicted amount of a SOM pool by a first-order decomposition model is ultimately determined by the ratio of the input rate and the decomposition rate coefficient. Figure 9 shows the distribution of the ratio of $\alpha_{NLF \rightarrow NLS}$ and k_{NLS}, which determines the total amount of the NLS pool. The spread for this ratio has become wider, despite the reduced spread of these parameters individually (Figure 2; c.f. also supporting information Figure S4). This is presumably caused by disagreement between the organic C and radiocarbon observations (see Figure 3 and section 4.1). This conflict means that for parameter changes in certain directions a reduced fit to the organic C data is compensated by an improved fit to the radiocarbon data. As a result, parameter sets that were previously assigned low likelihood due to poor fit to the organic carbon data may become more probable when the radiocarbon data is included, causing the predictive uncertainty for organic carbon to increase.

4.3. Methodological Constraints

The effective decomposition rate observations, as well as the radiocarbon activity of the heterotrophic respiration, were derived from measured fluxes from soil samples incubated in the lab, which may not be fully representative of conditions in the field. Simulated respiration rates were corrected for temperature and moisture maintained during the lab incubation, but disturbance of the soil samples may have stimulated respiration, leading to overestimated decomposition rates, which was not accounted for. The effective decomposition rates are underestimated for calibration wC14 (supporting information Figure S7), which suggests this problem is relevant here. Furthermore, the sample disturbance may also affect the radiocarbon signal of the respired CO_2 due to increased decomposition of old SOM [*Fontaine et al.*, 2007].

For the calibration, it was assumed that the average organic carbon stocks are in steady state and that radiocarbon is in steady state at the start of the simulation, in 1800. Furthermore, the uncertainty of the past forcing was not considered. The Hainich forest has a relatively constant and well-known history without major land use changes [*Wäldchen et al.*, 2013, section 2.1]. Nevertheless, as discussed in section 4.2, model

results and previous studies point to a positive soil carbon balance in the present. Furthermore, due to the long turnover times of NLS for calibration wC14, forcing fluctuations may affect soil carbon stocks for hundreds of years. Since the uncertainties resulting from deviations from the steady state and errors in the forcing data were not considered, it is likely that the spread of the posterior distribution is underestimated. Methods have been proposed to relax the steady state assumption [*Wutzler and Reichstein*, 2007; *Yeluripati et al.*, 2009; *Carvalhais et al.*, 2010] and consider forcing input errors [*Kavetski et al.*, 2006] which may be applied in future studies. For now it may be advisable to artificially increase the variance of the posterior distribution, if it is used as a prior for subsequent calibrations.

4.4. The Use of Radiocarbon Data for Constraining SOM Turnover and Transport

When radiocarbon data were omitted from the calibration, the observed C stocks and profile were well reproduced, but with a strongly overestimated turnover rate for the slowest SOM pool. This exemplifies the problem of an incorrect model producing correct results, as discussed in section 1. The obvious question is to what extent this leads to incorrect predictions and if avoiding these errors warrants the considerable cost and labour that comes with radiocarbon measurements? The future predictions for both calibration setups diverge for the transient simulations (Figure 7b). However, in relative terms, the differences are quite small (Figure 7a).

Nevertheless, we believe that SOM dynamics should be simulated based on accurate turnover rates, for several reasons. First, there is in general no guarantee that biases in the parameter estimates will be small enough that predictive errors are negligible. For other studies, the overestimation of the turnover rate may be more severe (c.f. the Loobos site in *Braakhekke et al.* [2013]). Several studies have shown that the partitioning of total SOM over different turnover fractions is highly relevant for transient predictions [*Telles et al.*, 2003; *Jones et al.*, 2005]. Furthermore, on longer time scales or in situations with more rapid environmental changes (e.g., land-use change or disturbances), overestimation of the transient response is more likely to occur. Second, as previously discussed, the response of decomposition to temperature may differ between SOM fractions [*Conant et al.*, 2011]. If this is the case, the distribution of total SOM over the different fractions is obviously highly relevant under conditions of climate change. Finally, consensus is emerging that the notion of SOM pools with fixed, intrinsic decomposition rates is incorrect. Rather, stabilization of SOM is the result of biological, physical, and chemical processes that may be reversible under the right conditions [*Schmidt et al.*, 2011]. Parametrization of these mechanisms and their effects on SOM decomposition requires accurate estimation of turnover rates.

Since C stock measurements do not contain information about the dynamic behavior of soil carbon, it is generally advisable to include one or more additional observations that directly relate to turnover when calibrating soil carbon models. This is corroborated by results of *Keenan et al.* [2013] who studied the value of different observations for calibration of an ecosystem model. They concluded that soil carbon turnover rates contributed greatly to improvement of model performance. Several candidate measurements are available, such as heterotrophic respiration rates (either in situ or in lab incubations), ^{13}C, and observations from chronosequences. However, in general radiocarbon is one of the best choices, particularly when dynamics of the slowest organic matter fractions are of interest [*Trumbore*, 2009]. Models that represent the complete vertical profile, such as SOMPROF, will generally require information on long time scale dynamics because of the very low turnover rates typical in the subsoil.

The fact that radiocarbon data yielded only marginal reduction of predictive uncertainty for certain variables in this study does not invalidate its use for constraining SOM transport and turnover. As discussed above, this is presumably related to the model's difficulty with fully fitting both the radiocarbon and C profile data. Hence, the radiocarbon data showed that predictive uncertainty for the C stocks was previously underestimated. It does not mean that the addition of this data led to a loss of information. Since Bayesian calibration constitutes conditioning of the model on (new) data, the uncertainty of the combined distribution of the predictions for all data streams cannot become higher.

Availability of soil radiocarbon data, although growing, is still limited [*Becker-Heidmann and Heidmann*, 2010], which hinders derivation of parameter sets for different soils and ecosystems. However, existing data may allow derivation of typical radiocarbon profiles for certain soils and ecosystems which could be used as observations. Furthermore, the Bayesian approach can be helpful in this respect since it allows results from calibrations for sites where radiocarbon data are available to be reused as prior distributions for sites where it is not.

5. Conclusions

The addition of radiocarbon data to the calibration had large effects on the posterior parameter distribution. Strongest changes occurred for the parameters controlling the formation and decomposition of the slowest organic matter pool, which were both strongly reduced. Additionally, the advection rate was reduced, resulting in more realistic predictions of SOM transport with the liquid phase. These results demonstrate that without constraint on long time scale turnover rates, the model may produce correct results based on incorrect parametrization.

Future projections show increasing carbon stocks initially, with levelling off, and—for the radiocarbon constrained model—carbon losses, near the end of the 21st century. The modified parameters had only small relative effects on carbon stock projections but led to markedly lower advective carbon losses and higher heterotrophic respiration. Radiocarbon data further led to a slight reduction of predictive uncertainty for the total carbon stock and a strong reduction for heterotrophic respiration.

Our results illustrate the risk of obtaining biased parameters, when available observations hold limited or no information on the dynamic behavior of SOM. Despite the absence of strong changes of the model predictions, we believe that radiocarbon is a valuable tool for constraining soil carbon models, particularly vertically explicit models such as SOMPROF.

Appendix A: Approximation of the Posterior Distribution Using Markov Chain Monte Carlo

Since the complexity of the model precludes analytical derivation of the posterior probability density function, the distribution was approximated with a Metropolis algorithm. This algorithm samples the posterior distribution by means of a Markov chain, which performs a random walk in parameter space. At each iteration i, proposals of the parameters θ^* are generated by taking a (semi-)random step from the current position θ^i. The model is run with the proposed parameter set and the unnormalized posterior probability density ($p(\theta)p(\mathbf{O}|\theta)$) of the proposal is evaluated. The proposal is subsequently accepted or rejected according to the Metropolis rule, which defines the chance for acceptance as

$$s = \min\left\{\frac{p(\mathbf{O}|\theta^*)p(\theta^*)}{p(\mathbf{O}|\theta^i)p(\theta^i)}, 1\right\}. \tag{A1}$$

The decision for acceptance or rejection is made using a random number from a uniform distribution on the unit interval. In case of acceptance, the chain moves to the position of the proposal; in case of rejection, the chain stays at the current position, which is thus sampled again.

The specific algorithm used here was DREAM(ZS) [*Laloy and Vrugt*, 2012], an adaptation of the DREAM (DiffeRential Evolution Adaptive Metropolis) algorithm which uses multiple chains in parallel and automatically adapts the scale and orientation of the proposal distribution. Eight chains were run for each calibration. The convergence of the chains was evaluated using the Gelman-Rubin index [*Gelman et al.*, 2004, Chap. 11], which is proportional to the ratio of the between-chain variance and the within-chain variance, and declines to 1 when the chains converge on the same distribution. All chains were run until the convergence index was $\leq$ 1.01 for all parameters, with at least 100,000 iterations per chain. After the runs, a variable number of iterations was removed from the start of each chain (the "burn-in"). Next, the remaining samples for each chain were merged and thinned to 10,000 iterations for analysis by selecting iterations in regular intervals. Marginal probability distributions depicted in Figure 2 were derived using kernel density estimation [*Bowman and Azzalini*, 1997]. For the model results depicted in Figures 3–5, 5000 simulations were made based on parameters sets from the Monte Carlo samples. The projection simulations were based on 500 samples. These samples were selected in regular intervals (i.e., every n^{th} sample was selected) from the Markov chains. This assures that dependence between the selected samples is minimal.

Acknowledgments
We are indebted to Thomas Wutzler and Nuno Carvalhais for advice on the methods. Additionally we thank three anonymous reviewers for their constructive comments on the manuscript draft. This work was supported by the ERC starting grant QUASOM (ERC-2007-StG-208516).

References

Arora, V. K., and H. D. Matthews (2009), Characterizing uncertainty in modeling primary terrestrial ecosystem processes, *Global Biogeochem. Cycles*, *23*, GB2016, doi:10.1029/2008GB003398.

Baisden, W. T., R. Amundson, D. L. Brenner, a. C. Cook, C. Kendall, and J. W. Harden (2002), A multiisotope C and N modeling analysis of soil organic matter turnover and transport as a function of soil depth in a California annual grassland soil chronosequence, *Global Biogeochem. Cycles*, *16*(4), 82–1–82–26, doi:10.1029/2001GB001823.

Becker-Heidmann, P., and P. Heidmann (2010), A new attempt to establish the International Radiocarbon Soils Database (IRSDB), *Radiocarbon*, *52*(3), 1405–1410.
Beven, K. (2006), A manifesto for the equifinality thesis, *J. Hydrol.*, *320*(1-2), 18–36, doi:10.1016/j.jhydrol.2005.07.007.
Bowman, A., and A. Azzalini (1997), *Applied Smoothing Techniques for Data Analysis: The Kernel Approach With S-Plus Illustrations*, Oxford University Press, Oxford.
Braakhekke, M. C., C. Beer, M. R. Hoosbeek, M. Reichstein, B. Kruijt, M. Schrumpf, and P. Kabat (2011), SOMPROF: A vertically explicit soil organic matter model, *Ecol. Modell.*, *222*, 1712–1730.
Braakhekke, M. C., et al. (2013), Modeling the vertical soil organic matter profile using Bayesian parameter estimation, *Biogeosciences*, *10*(1), 399–420, doi:10.5194/bg-10-399-2013.
Brovkin, V., T. Raddatz, C. H. Reick, M. Claussen, and V. Gayler (2009), Global biogeophysical interactions between forest and climate, *Geophys. Res. Lett.*, *36*, L07405, doi:10.1029/2009GL037543.
Carvalhais, N., M. Reichstein, P. Ciais, G. J. Collatz, M. D. Mahecha, L. Montagnani, D. Papale, S. Rambal, and J. Seixas (2010), Identification of vegetation and soil carbon pools out of equilibrium in a process model via eddy covariance and biometric constraints, *Global Change Biol.*, *16*(10), 2813–2829, doi:10.1111/j.1365-2486.2010.02173.x.
Chabbi, A., I. Kögel-Knabner, and C. Rumpel (2009), Stabilised carbon in subsoil horizons is located in spatially distinct parts of the soil profile, *Soil Biol. Biochem.*, *41*(2), 256–261, doi:10.1016/j.soilbio.2008.10.033.
Christensen, J. H., F. Boberg, O. B. Christensen, and P. Lucas-Picher (2008), On the need for bias correction of regional climate change projections of temperature and precipitation, *Geophys. Res. Lett.*, *35*(20), L20709, doi:10.1029/2008GL035694, http://www.ensembles-eu.org/.
Conant, R. T., et al. (2011), Temperature and soil organic matter decomposition rates—Synthesis of current knowledge and a way forward, *Global Change Biology*, *17*(11), 3392–3404, doi:10.1111/j.1365-2486.2011.02496.x.
Cramer, W., et al. (2001), Global response of terrestrial ecosystem structure and function to CO_2 and climate change: Results from six dynamic global vegetation models, *Global Change Biol.*, *7*(4), 357–373, doi:10.1046/j.1365-2486.2001.00383.x.
Davidson, E., and I. Janssens (2006), Temperature sensitivity of soil carbon decomposition and feedbacks to climate change, *Nature*, *440*(7081), 165–173, doi:10.1038/nature04514.
Dee, D., et al. (2011), The ERA-interim reanalysis: Configuration and performance of the data assimilation system, *Q. J. R. Meteorolog. Soc.*, *137*(656), 553–597.
Ekici, A., C. Beer, S. Hagemann, and C. Hauck (2013), Improved soil physics for simulating high latitude permafrost regions by the JSBACH terrestrial ecosystem model, *Geosci. Model Dev. Discuss.*, *6*(2), 2655–2698, doi:10.5194/gmdd-6-2655-2013.
Elzein, A., and J. Balesdent (1995), Mechanistic simulation of vertical distribution of carbon concentrations and residence times in soils, *Soil Sci. Soc. Am. J.*, *59*(5), 1328–1335.
Eusterhues, K., C. Rumpel, M. Kleber, and I. Kögel-Knabner (2003), Stabilisation of soil organic matter by interactions with minerals as revealed by mineral dissolution and oxidative degradation, *Org. Geochem.*, *34*(12), 1591–1600.
Falloon, P., P. Smith, K. Coleman, and S. Marshall (2000), How important is inert organic matter for predictive soil carbon modelling using the Rothamsted carbon model?, *Soil Biol. Biochem.*, *32*(3), 433–436, doi:10.1016/S0038-0717(99)00172-8.
Federer, C. A., D. E. Turcotte, and C. T. Smith (1993), The organic fraction–bulk density relationship and the expression of nutrient content in forest soils, *Can. J. For. Res.*, *23*(6), 1026–1032.
Fierer, N., A. Allen, J. Schimel, and P. Holden (2003), Controls on microbial CO_2 production: A comparison of surface and subsurface soil horizons, *Global Change Biol.*, *9*(9), 1322–1332, doi:10.1046/j.1365-2486.2003.00663.x.
Fontaine, S., S. Barot, P. Barre, N. Bdioui, B. Mary, and C. Rumpel (2007), Stability of organic carbon in deep soil layers controlled by fresh carbon supply, *Nature*, *450*(7167), 277–280.
Friedlingstein, P., et al. (2006), Climate-carbon cycle feedback analysis: Results from the C^4MIP model intercomparison, *J. Clim.*, *19*(14), 3337–3353.
Fujiyoshi, R., and S. Sawamura (2004), Mesoscale variability of vertical profiles of environmental radionuclides (K-40, Ra-226, Pb-210 and Cs-137) in temperate forest soils in Germany, *Sci. Total Environ.*, *320*(2-3), 177–188.
Gaudinski, J., S. Trumbore, E. Davidson, and S. Zheng (2000), Soil carbon cycling in a temperate forest: Radiocarbon-based estimates of residence times, sequestration rates and partitioning of fluxes, *Biogeochemistry*, *51*(1), 33–69, doi:10.1023/A:1006301010014.
Gelman, A., J. B. Carlin, S. Stern, and D. B. Rubin (2004), *Bayesian Data Analysis*, Chapman & Hall/CRC Press, Boca Raton, Florida.
Hahn, V., and N. Buchmann (2004), A new model for soil organic carbon turnover using bomb carbon, *Global Biogeochem. Cycles*, *18*(1), GB1019, doi:10.1029/2003GB002115.
Hua, Q., and M. Barbetti (2004), Review of tropospheric bomb C-14 data for carbon cycle modeling and age calibration purposes, *Radiocarbon*, *46*(3), 1273–1298.
Hungate, B., J. Dukes, M. Shaw, Y. Luo, and C. Field (2003), Nitrogen and climate change, *Science*, *302*(5650), 1512–1513, doi:10.1126/science.1091390.
IUSS Working Group WRB (2007), World reference base for soil resources 2006, first update 2007, *World Soil Resources Reports No. 103*, FAO, Rome.
Iversen, C. M. (2010), Digging deeper: Fine-root responses to rising atmospheric CO_2 concentration in forested ecosystems, *New Phytol.*, *186*(2), 346–357, doi:10.1111/j.1469-8137.2009.03122.x.
Janssens, I. A., et al. (2010), Reduction of forest soil respiration in response to nitrogen deposition, *Nat. Geosci.*, *3*(5), 315–322, doi:10.1038/ngeo844.
Jenkinson, D., and K. Coleman (1994), Calculating the annual input of organic matter to soil from measurements of total organic-carbon and radiocarbon, *Eur. J. Soil Sci.*, *45*(2), 167–174.
Jenkinson, D. S., and K. Coleman (2008), The turnover of organic carbon in subsoils. Part 2. Modelling carbon turnover, *Eur. J. Soil Sci.*, *59*(2), 400–413.
Jones, C., and P. Falloon (2009), Sources of uncertainty in global modelling of future soil organic carbon storage, in *Uncertainties in Environmental Modelling and Consequences for Policy Making, NATO Science for Peace and Security Series C-Environmental Security*, edited by P. Baveye, M. Laba, and J. Mysiak, pp. 283–315, Springer, Netherlands.
Jones, C., C. McConnell, K. Coleman, P. Cox, P. Falloon, D. Jenkinson, and D. Powlson (2005), Global climate change and soil carbon stocks; predictions from two contrasting models for the turnover of organic carbon in soil, *Global Change Biol.*, *11*(1), 154–166, doi:10.1111/j.1365-2486.2004.00885.x.
Kaiser, K., and K. Kalbitz (2012), Cycling downwards—Dissolved organic matter in soils, *Soil Biol. Biochem.*, *52*, 29–32, doi:10.1016/j.soilbio.2012.04.002.

Kavetski, D., G. Kuczera, and S. W. Franks (2006), Bayesian analysis of input uncertainty in hydrological modeling: 1. Theory, *Water Resour. Res.*, *42*(3), W03407, doi:10.1029/2005WR004368.

Keenan, T. F., E. A. Davidson, J. W. Munger, and A. D. Richardson (2013), Rate my data: Quantifying the value of ecological data for the development of models of the terrestrial carbon cycle, *Ecol. Appl.*, *23*(1), 273–286.

Kindler, R., et al. (2011), Dissolved carbon leaching from soil is a crucial component of the net ecosystem carbon balance, *Global Change Biol.*, *17*(2), 1167–1185, doi:10.1111/j.1365-2486.2010.02282.x.

Knohl, A., E. Schulze, O. Kolle, and N. Buchmann (2003), Large carbon uptake by an unmanaged 250-year-old deciduous forest in Central Germany, *Agric. For. Meteorol.*, *118*(3-4), 151–167, doi:10.1016/S0168-1923(03)00115-1.

Knorr, W. (2000), Annual and interannual CO_2 exchanges of the terrestrial biosphere: Process-based simulations and uncertainties, *Global Ecol. Biogeogr.*, *9*(3), 225–252.

Koarashi, J., W. C. Hockaday, C. A. Masiello, and S. E. Trumbore (2012), Dynamics of decadally cycling carbon in subsurface soils, *J. Geophys. Res.*, *117*, G03033, doi:10.1029/2012JG002034.

Koven, C. D., W. J. Riley, Z. M. Subin, J. Y. Tang, M. S. Torn, W. D. Collins, G. B. Bonan, D. M. Lawrence, and S. C. Swenson (2013), The effect of vertically resolved soil biogeochemistry and alternate soil C and N models on C dynamics of CLM4, *Biogeosciences*, *10*(11), 7109–7131, doi:10.5194/bg-10-7109-2013.

Kutsch, W., T. Persson, M. Schrumpf, F. Moyano, M. Mund, S. Andersson, and E.-D. Schulze (2010), Heterotrophic soil respiration and soil carbon dynamics in the deciduous Hainich forest obtained by three approaches, *Biogeochemistry*, *100*, 1–17.

Laloy, E., and J. A. Vrugt (2012), High-dimensional posterior exploration of hydrologic models using multiple-try DREAM(ZS) and high-performance computing, *Water Resour. Res.*, *48*, W01526, doi:10.1029/2011WR010608.

Levin, I., and B. Kromer (2004), The tropospheric (CO_2)-C-14 level in mid-latitudes of the northern hemisphere (1959–2003), *Radiocarbon*, *46*(3), 1261–1272.

Lloyd, J., and J. A. Taylor (1994), On the temperature dependence of soil respiration, *Funct. Ecol.*, *8*(3), 315–323.

Manzoni, S., and A. Porporato (2009), Soil carbon and nitrogen mineralization: Theory and models across scales, *Soil Biol. Biochem.*, *41*(7), 1355–1379, doi:10.1016/j.soilbio.2009.02.031.

Mead, R. (1965), A generalised logit-normal distribution, *Biometrics*, *21*(3), 721–732.

Medlyn, B., A. Robinson, R. Clement, and R. McMurtrie (2005), On the validation of models of forest CO_2 exchange using eddy covariance data: Some perils and pitfalls, *Tree Physiol.*, *25*(7), 839–857.

Meinshausen, M., et al. (2011), The RCP greenhouse gas concentrations and their extensions from 1765 to 2300, *Clim. Change*, *109*(1-2), 213–241.

Michalzik, B., E. Tipping, J. Mulder, J. Lancho, E. Matzner, C. Bryant, N. Clarke, S. Lofts, and M. Esteban (2003), Modelling the production and transport of dissolved organic carbon in forest soils, *Biogeochemistry*, *66*(3), 241–264, doi:10.1023/B:BIOG.0000005329.68861.27.

Perruchoud, D., F. Joos, A. Fischlin, I. Hajdas, and G. Bonani (1999), Evaluating timescales of carbon turnover in temperate forest soils with radiocarbon data, *Global Biogeochem. Cycles*, *13*(2), 555–573, doi:10.1029/1999GB900003.

Petersen, B., J. Berntsen, S. Hansen, and L. Jensen (2005), CN-SIM - a model for the turnover of soil organic matter. I. Long-term carbon and radiocarbon development, *Soil Biol. Biochem.*, *37*(2), 359–374, doi:10.1016/j.soilbio.2004.08.006.

Piani, C., G. Weedon, M. Best, S. Gomes, P. Viterbo, S. Hagemann, and J. Haerter (2010), Statistical bias correction of global simulated daily precipitation and temperature for the application of hydrological models, *J. Hydrol.*, *395*(3), 199–215.

Press, W. H., S. A. Teukolsky, W. T. Vetterling, and B. P. Flannery (1996), *Numerical Recipes in Fortran 90 (2nd Ed.): The Art of Parallel Scientific Computing*, Cambridge Univ. Press, New York.

Raddatz, T. J., C. H. Reick, W. Knorr, J. Kattge, E. Roeckner, R. Schnur, K.-G. Schnitzler, P. Wetzel, and J. Jungclaus (2007), Will the tropical land biosphere dominate the climate-carbon cycle feedback during the twenty-first century?, *Clim. Dyn.*, *29*(6), 565–574, doi:10.1007/s00382-007-0247-8.

Reimer, P., et al. (2004), IntCal04 terrestrial radiocarbon age calibration, 0–26 cal kyr BP, *Radiocarbon*, *46*(3), 1029–1058.

Rumpel, C., I. Kögel-Knabner, and F. Bruhn (2002), Vertical distribution, age, and chemical composition of organic, carbon in two forest soils of different pedogenesis, *Org. Geochem.*, *33*(10), 1131–1142.

Rumpel, C., A. Chabbi, and B. Marschner (2012), Carbon storage and sequestration in subsoil horizons: Knowledge, gaps and potentials, in *Recarbonization of the Biosphere: Ecosystems and the Global Carbon Cycle*, edited by R. Lal, K. Lorenz, and R. Hüttl, pp. 445–464, Springer, Netherlands.

Schmidt, M. W. I., et al. (2011), Persistence of soil organic matter as an ecosystem property, *Nature*, *478*(7367), 49–56, doi:10.1038/nature10386.

Schrumpf, M., E. D. Schulze, K. Kaiser, and J. Schumacher (2011), How accurately can soil organic carbon stocks and stock changes be quantified by soil inventories?, *Biogeosciences*, *8*(5), 1193–1212, doi:10.5194/bg-8-1193-2011.

Schrumpf, M., K. Kaiser, G. Guggenberger, T. Persson, I. Kögel-Knabner, and E.-D. Schulze (2013), Storage and stability of organic carbon in soils as related to depth, occlusion within aggregates, and attachment to minerals, *Biogeosciences*, *10*(3), 1675–1691, doi:10.5194/bg-10-1675-2013.

Sierra, C. A., S. E. Trumbore, E. A. Davidson, S. D. Frey, K. E. Savage, and F. M. Hopkins (2012), Predicting decadal trends and transient responses of radiocarbon storage and fluxes in a temperate forest soil, *Biogeosciences*, *9*(8), 3013–3028, doi:10.5194/bg-9-3013-2012.

Sitch, S., et al. (2008), Evaluation of the terrestrial carbon cycle, future plant geography and climate-carbon cycle feedbacks using five Dynamic Global Vegetation Models (DGVMS), *Global Change Biol.*, *14*(9), 2015–2039.

Stuiver, M., and H. Polach (1977), Reporting of C-14 data—Discussion, *Radiocarbon*, *19*(3), 355–363.

Stuiver, M., P. Reimer, and T. Braziunas (1998), High-precision radiocarbon age calibration for terrestrial and marine samples, *Radiocarbon*, *40*(3), 1127–1151.

Tang, J., and Q. Zhuang (2008), Equifinality in parameterization of process-based biogeochemistry models: A significant uncertainty source to the estimation of regional carbon dynamics, *J. Geophys. Res.*, *113*(G4), G04010, doi:10.1029/2008JG000757.

Tefs, C., and G. Gleixner (2012), Importance of root derived carbon for soil organic matter storage in a temperate old-growth beech forest: Evidence from C, N and ^{14}C content, *For. Ecol. Manage.*, *263*(0), 131–137, doi:10.1016/j.foreco.2011.09.010.

Telles, E. d. C. C., P. B. de Camargo, L . A. Martinelli, S. E. Trumbore, E. S. da Costa, J. Santos, N. Higuchi, and R. C. Oliveira (2003), Influence of soil texture on carbon dynamics and storage potential in tropical forest soils of Amazonia, *Global Biogeochem. Cycles*, *17*(2), 1040, doi:10.1029/2002GB001953.

Todd-Brown, K. E. O., J. T. Randerson, W. M. Post, F. M. Hoffman, C. Tarnocai, E. A. G. Schuur, and S. D. Allison (2013), Causes of variation in soil carbon simulations from CMIP5 earth system models and comparison with observations, *Biogeosciences*, *10*(3), 1717–1736, doi:10.5194/bg-10-1717-2013.

Trumbore, S. (2009), Radiocarbon and soil carbon dynamics, *Annu. Rev. Earth Planet. Sci.*, *37*, 47–66, doi:10.1146/annurev.earth.36.031207.124300.

Trumbore, S., E. Davidson, P. Decamargo, D. Nepstad, and L. Martinelli (1995), Belowground cycling of carbon in forests and pastures of eastern Amazonia, *Global Biogeochem. Cycles*, *9*(4), 515–528, doi:10.1029/95GB02148.

van Dam, D., E. Veldkamp, and N. van Breemen (1997), Soil organic carbon dynamics: Variability with depth in forested and deforested soils under pasture in Costa Rica, *Biogeochemistry*, *39*(3), 343–375, doi:10.1023/A:1005880031579.

Wäldchen, J., E.-D. Schulze, I. Schoening, M. Schrumpf, and C. Sierra (2013), The influence of changes in forest management over the past 200 years on present soil organic carbon stocks, *For. Ecol. Manage.*, *289*, 243–254, doi:10.1016/j.foreco.2012.10.014.

Weedon, G., S. Gomes, P. Viterbo, H. Österle, J. Adam, N. Bellouin, O. Boucher, and M. Best (2010), The watch forcing data 1958–2001: A meteorological forcing dataset for land surface and hydrological models, *WATCH Technical Report No. 22*, Centre for Ecology and Hydrology.

Wieder, W. R., G. B. Bonan, and S. D. Allison (2013), Global soil carbon projections are improved by modelling microbial processes, *Nature Clim. Change*, *3*(10), 909–912, doi:10.1038/nclimate1951.

Wutzler, T., and M. Reichstein (2007), Soils apart from equilibrium—Consequences for soil carbon balance modelling, *Biogeosciences*, *4*(1), 125–136.

Yeluripati, J. B., M. van Oijen, M. Wattenbach, A. Neftel, A. Ammann, W. J. Parton, and P. Smith (2009), Bayesian calibration as a tool for initialising the carbon pools of dynamic soil models, *Soil Biol. Biochem.*, *41*(12), 2579–2583, doi:10.1016/j.soilbio.2009.08.021.